Spin-orbit splitting of quantum well states in *n*-monolayer Ir/Au(111) heterostructures

I. V. Silkin,[1,*] Yu. M. Koroteev,[1,2,3] V. M. Silkin,[4,5,6] and E. V. Chulkov[4,5,7,3]

[1]*Tomsk State University, pr. Lenina 36, 634050 Tomsk, Russia*

[2]*Institute of Strength Physics and Materials Science, Siberian Branch, Russian Academy of Sciences, 634055 Tomsk, Russia*

[3]*St. Petersburg State University, 198504 St. Petersburg, Russia*

[4]*Departamento de Física de Materiales, Facultad de Ciencias Químicas, Universidad del País Vasco UPV/EHU, Apartado 1072, 20080 San Sebastián/Donostia, Basque Country, Spain*

[5]*Donostia International Physics Center, P. de Manuel Lardizabal 4, 20018 San Sebastián/Donostia, Basque Country, Spain*

[6]*IKERBASQUE, Basque Foundation for Science, 48013 Bilbao, Basque Country, Spain*

[7]*Centro de Fisica de Materiales, Centro Mixto CSIC-UPV/EHU, P. de Manuel Lardizabal, 5, 20018 San Sebastian/Donostia, Basque Country, Spain*

(Received 9 October 2019; revised manuscript received 24 April 2020; accepted 11 May 2020; published 5 June 2020)

The effect of spin-orbit coupling on quantum well states (QWSs) in atomically thin Ir adlayers deposited on the Au(111) substrate is studied in the framework of the density functional theory. Varying the Ir film thickness from 1 to 3 atomic layers, we find numerous Ir-derived QWSs, which are mainly of *d* character. The resulting band dispersion of QWSs appearing around the surface Brillouin zone center in a wide Au(111) energy gap is analyzed in the framework of the Rashba model. In all such QWSs, the fitted values of the Rashba parameter exceed 2 eV Å. The maximal value of 6.4 eV Å was obtained for the 1-monolayer-Ir/Au(111) system. We explain such large spin splitting by hybridization between different QWSs. Strong enhancement is observed in the density of electronic states at the surface in the energy region around the Fermi level caused by these QWSs.

DOI: 10.1103/PhysRevB.101.235409

I. INTRODUCTION

In crystals without inversion symmetry a twofold Kramer's degeneracy of the electron energy bands protected by time-reversal symmetry is lifted. As a result, these bands are split into two sets by the spin-orbit coupling (SOC) and each of these bands is characterized by the momentum and spin [1,2]. This effect constitutes a basis for a wide variety of phenomena realized in condensed matter systems [3–5]. In particular, at surfaces and interfaces where the crystal symmetry is broken, the phenomenon known as Rashba spin-orbit coupling takes place in the two-dimensional electron states [6,7]. The research fields exploiting this spin-orbit interaction have received great attention since, besides the fascinating physics, promising materials suitable for room-temperature spin-based device applications can be developed.

One of the directions in the running investigations is the search for materials characterized by a large strength of SOC, which can be quantified by the Rashba parameter α_R. This parameter determines the linear term in the resulting energy band dispersions from the Rashba point, where the two bands intersect. Several routs in finding the systems with the largest SOC parameter were exploited. For instance, the spin-orbit splitting of the energy bands in the metallic systems is significantly larger in comparison to the conventional semiconductor systems. A large splitting of the surface states due to the spin-orbit interaction was first discovered at the noble metal surfaces [8–10].

To enhance α_R, an obvious choice is to use the heavier elements like lead and bismuth. Thus, strong Rashba spin-orbit splitting of the surface-state bands was found on low-index Bi surfaces [11,12] and in ultrathin Bi films deposited on a Si(111) surface [13,14]. Exceptionally large spin-orbit Rashba splitting was observed in the surface states realized in ordered surface alloys formed by heavy elements like Bi or Pb on the surfaces of noble metals Ag or Cu [15–17]. In such surface alloys the surface state energies and spin-orbit splitting can be tuned by changing the composition parameters. Even larger splitting was found in the surface and bulk states of layered polar semiconductors, like BiTeI [18–21], which is about one order of magnitude larger than that in the conventional semiconductor quantum wells [22,23]. In the calculations for organic-inorganic perovskite compounds (OIPCs), the Rashba parameters in a wide range from <0.1 to almost 10 eV Å were obtained [24]. The measurements using the angle-resolved photoemission spectroscopy found Rashba parameters α_R of 7 ± 1 and 11 ± 4 eV Å [25].

Spin-orbit interaction has also received great attention in the field of topological insulators [26–30]. In addition to topological surface state in the fundamental energy gap, an unoccupied Dirac cone like surface state was found in the local energy gap of the topological insulators [31–33].

The SOC effects are greatly enhanced in the systems of reduced dimensions. Therefore a natural way to induce a giant spin-orbit splitting consists in exploiting the quantum-well states (QWSs) in atomically thin films that originate

*igor_silkin83@mail.ru

from a quantization of the electronic states in the surface-perpendicular direction [34–36]. For instance, the SOC effect on the d and s-p QWSs in Au adlayers on W(110) and Mo(110) was studied experimentally and theoretically [37]. The QWSs observed in a Bi monolayer (ML) adsorbed on Cu(111) [17] show a remarkably strong Rashba spin-orbit splitting reaching the Rashba parameter between $\alpha_R = 1.5$ and 2.5 eV Å. These QWSs are totally unoccupied and located at about 2 eV above the Fermi level (E_F).

Of a special interest are the quantum states with energies close to E_F. Such kind of states can be introduced by, e.g., transition metal atoms. Theoretically, Wu and Li showed [38] that giant SOC in the electronic states close to E_F can occur in thin free-standing Ir films with thickness of few atomic layers when one of the sides is covered by a H ML. Even though the spin-orbit interaction in H atoms is extremely weak, the H-Ir interaction induces such a splitting by breaking the inversion symmetry of the film. A deposition of a graphene ML on the H-terminated 3ML Ir(111) results in a slight shift of the energies of the Ir electronic states [38]. This correlates with a small effect on the Ir(111) surface state dispersion upon the graphene deposition observed in photoemission [39]. An extensive first-principles study of the adsorption of Ir on the Au(111) surface considering the Ir coverage from 1/9 up to one ML was performed by Freire *et al.* [40]. However, the details of electronic structure were not reported in that publication.

On the experimental side, recently the Ir-Au bimetallic systems created by deposition of Ir atoms on Au substrates have started to attract attention as promising candidates for automotive exhaust catalysis. However, the existing experimental work in the field of catalysis was focused on synthesis of small Ir nanoparticles (NPs) which offer maximum surface/volume ratios. Thus Ahn *et al.* [41] found that at the sub-ML deposition rate the Ir islands of ≈(2 to 3) nm in diameter grow on the Au surface. Upon increase of Ir coverage, the dense pyramidal Ir islands of a thickness equivalent to 8 Ir MLs formed on the Au(111) surface. The interface was atomically sharp in both cases. In the experiment by Štrbac *et al.* [42] after short deposition time, a coverage of the Au(111) surface with Ir was achieved with deposited islands of one to four MLs high. The lateral size of the deposited Ir islands ranged from 10 to 25 nm. For longer deposition times, the lateral size of Ir islands ranged from 25 to 50 nm without an increase in the deposit height. However, exact atomic distribution in NPs grown in these and other publications [43–50] was not studied.

Up to now, the Ir/Au(111) systems were grown in inherently dirty electrodeposition processes where it is difficult to control the film morphology. On the other hand, to explore the Rashba effects in atomically thin Ir films on Au(111) one would need to grow such films in a well-controlled ultrahigh vacuum environment. However, it might be difficult to realize the formation of Ir films on Au(111) since in the density-functional calculations the Ir atoms on the Au(111) surface prefer to localize beneath the top Au atoms [40]. At the same time, experimentally Zhang *et al.* [51,52] detected movement of deposited Ir atoms into bulk Au at temperatures above 400 K only. Moreover, they speculated that the as deposited 3D Ir islands may change to a more uniform morphology after gentle heating below 400 K. This suggests that it might be possible to create metastable atomically thin nML-Ir/Au(111) systems employing a substrate, cold enough to inhibit alloying or three-dimensional (3D) island formation [53].

In this work, we study the electronic structure of the nML-Ir/Au(111) heterostructures with a number n of Ir atomic layers ranging from one to three. The number of valence electrons in Ir is less by one than in Pt. Consequently, the energy positions of the Ir QWSs around E_F are shifted upward in comparison with the nML-Pt/Au(111) system studied recently [54], which offers additional possibities in engineering the electronic states in such bimetallic systems. The dispersion shape and properties of the Ir-related QWSs as well as the layer-resolved density of states (LDOS) are analyzed. The impact of the spin-orbit interaction on these states is quantified by analyzing the electronic structure and LDOS obtained with and without spin-orbit coupling (WSOC) included. In particular, we analyze the SOC effect on the Ir-derived QWSs of d character in the framework of the Rashba model.

The rest of the paper is organized as follows. In Sec. II, a brief description of the methods used and some computational details are given. In Sec. III, we present the electronic structure of the systems under study. The summary and conclusions are presented in Sec. IV.

II. CALCULATION METHODS

The calculations were performed within the framework of the density functional theory formalism by the projector augmented wave method employing a pseudopotential scheme implemented in the VASP code [55,56]. For the description of the exchange-correlation effects, the local density approximation in the Ceperley-Alder parametrization was used [57].

The configurations $5d^{10}6s^1$ and $5d^7 6s^2$ were used for the valence electrons in Au and Ir, respectively. Self-consistent electron density was determined by using a Monkhorst-Pack scheme [58] with a $11 \times 11 \times 1$ grid of $\mathbf{k}_\parallel$ points in the surface Brillouin zone (SBZ). For all calculations, we used the criterion of convergence with respect to the total energy to 10^{-8} eV.

The optimized bulk lattice parameters are $a_0 = 4.04$ Å for Au and $a_0 = 3.82$ Å for Ir. The calculated lattice constants are in good agreement with the experimentally determined values $a_0 = 4.045$ Å for Au [59] and $a_0 = 3.8341$ Å for Ir [60]. The clean Ir(111) and Au(111) surfaces of a semifinite crystal were simulated with a 23 layers film. The same number of layers was employed for the description of the gold substrate in the case of the nML-Ir/Au(111) systems, where the Ir adlayers consisting of n atomic layers were placed on both sides of the slab. The in-plane lattice parameter for the Ir adlayers was chosen to be equal to the Au bulk constant. For each system, we performed optimization of the vertical atomic positions in the Ir adsorbate layers and four outermost layers of the Au substrate on each side of the film. Fifteen internal Au atomic layers were kept in their bulk positions.

It is known that heterostructures based on atomically thin adlayers may have complex behavior depending on the concentration of the adatoms. Especially complex atomic structure can be realized for sub-ML and 1 ML adlayer thicknesses. Frequently, an adlayer is formed, while in other cases the adsorbate forms an ordered ML beneath the surface atomic

layer of the substrate. Regarding the Ir adsorption on the flat Au(111) surface, from the study of sub-ML and 1 ML Ir adsorption on the Au(111) surface Freire *et al.* [40] concluded that the top gold ML prefers to segregate above the Ir ML. The same conclusion was derived from the calculations of the segregation energy in the 3ML Au-Ir-Ir and Ir-Au-Ir systems [61]. Such behavior can be explained by large positive surface segregation energy for the Ir impurity on the Au(111) surface calculated by Ruban *et al.* [62]. Based on this theoretical work, here we studied the electronic structure of the 1ML-Ir/Au(111) heterostructure for two vertical positions of the Ir ML: on top of the Au(111) surface and beneath the surface Au atomic layer. In the case of 2 and 3 Ir MLs the on-top position of the Ir adlayer was chosen.

To reveal the SOC impact introduced in the electronic states of the nML-Ir/Au(111) systems, the band structure is calculated with and without spin-orbit coupling included. In this work, we concentrate on the Ir-induced QWSs around the SBZ center. For the analysis of its spin-orbit splitting, we employ a simple model accounting for SOC by the Rashba Hamiltonian [2,6,7]. The parameters of this model are the effective mass m^* and the Rashba parameter α_R. The band maximum (minimum) is shifted by SOC from $\mathbf{k}_\parallel = 0$ (denoted as a $\overline{\Gamma}$ point in the SBZ) by $k_\parallel^0$ and found at an energy of E_0 with respect to the position at $\overline{\Gamma}$, and the Rashba parameter is defined as $\alpha_R = 2E_0/k_0$. An alternative way consists in the determination of the linear dispersion term of the spin-orbit split band pair in the vicinity of the Rashba point [63].

III. RESULTS AND DISCUSSION

A. Clean Au(111) and Ir(111) surfaces

The electronic structure of a clean Au(111) surface was previously studied in detail both experimentally and theoretically in numerous publications. In this work, we base on the one reported in Fig. 4 of Ref. [54]. In gold, the $5d$ valence electronic bands are completely occupied and reside at energies below about -2 eV and the states around E_F are of the mainly s-p character. An attractive feature of the Au(111) surface electronic structure is the presence of a wide energy gap in the bulk spectrum around the SBZ center at energies above ≈ -1.4 eV. In this energy gap there exits a surface state of s-p character with a parabolic-like dispersion and energy of ≈ -0.5 eV at the $\overline{\Gamma}$ point with respect to the Fermi level. Away from the $\overline{\Gamma}$ point this surface state disperses upward, crosses E_F and can be traced up to about 1 eV above E_F. This state is frequently referred to as a Shockley surface state. Its wave function is localized in the surface region with substantial expansion to the vacuum side [64]. Such spatial localization of this surface state can explain its disappearance upon the deposition of various adlayers. In particular, it occurs in the case of the alkali atom ultra-thin coverage on Cu (111) [65,66] and Pt(111) [66] as well as in the case of the Pt thin film adsorption [54]. The same behavior we observe in the present case of Ir adsorption on Au(111).

The spin-orbit coupling has a strong impact on the dispersion of the Au(111) Shockley surface state [54,67]. Its energy is shifted by several tens meV downward upon the inclusion of spin-orbit interaction in the calculation. Moreover, this state experiences notable Rashba spin-orbit splitting, which can be described with a splitting coefficient (Rashba parameter) $\alpha_R \approx 0.35$ eV Å [8].

A number of other occupied surface states of d character can be found in Au(111) below -2 eV. These states experience notable splitting upon the inclusion of spin-orbit interaction. Their characteristics obtained in our calculation are close to those found in other density-functional calculations [9,10,67–70] and agree with the photoemission experiment data [68].

In order to better understand the electronic structure of atomically thin Ir films and the impact by the Au substrate, in Fig. 1, we present the electronic structure of a clean Ir(111) surface. The electronic structure calculated with taking into account the spin-orbit interaction is reported in Fig. 1(a). Here, one can see that at energies below $\approx$1.5 eV the electronic states are of mainly d character. Above this energy, the electronic states have essentially s-p character. In the center of the SBZ there is an energy gap in the unoccupied part of the spectrum. Its bottom is at 1.23 eV, with the border having a parabolic-like upward dispersion. A similar energy gap exists on the (111) face of noble and other transition metals. However, in contrast to the noble metal surfaces, Pd(111), and Pt(111) [71–76], this gap in Ir(111) does not support a Shockley-like surface state. We explain this fact by a symmetry of the lower edge of the energy gap which has d character in Ir(111). For instance, in the (111) noble metal surfaces the symmetry of the lower edge is of a p type. As a result, the condition of a "p-s" inverted energy gap for the existence of a Shockley surface state is fulfilled [77]. In Ir(111), the symmetry of this gap is "d-s". This correlates with the absence of such a state on the Os(0001) surface, where a similar d-s energy gap exists [78]. In general, our calculated electronic structure of Ir(111) is very close to that calculated by Dal Corso [79]. Furthermore, the calculated data are in agreement with the photoemission experiments [80,81].

Several surface states can be found in Fig. 1(a) in the unoccupied part at finite wave vectors. The majority of them have resonance character. With the spin-orbit interaction included, the majority of these states reduce its localization at the surface as can be deduced from the comparison with Fig. 1(b), where the Ir(111) electronic structure obtained without the inclusion of the spin-orbit term is reported. With SOC included, only the surface state located in close vicinity to E_F along the $\overline{MK}$ direction enhances its surface character due to the shift into the energy gap interior. Its energy position and dispersion are very close to the data of the photoemission experiment [82] that found this state at E_F at the $\overline{K}$ point locating and dispersing downward with changing the wave vector from $\overline{K}$ toward the $\overline{\Gamma}$ point.

In the occupied part of the SOC electronic structure reported in Fig. 1(a), we find several surface and resonance states with strong localization at the surface owing to its d character. In particular, in the vicinity of the $\overline{\Gamma}$ point just below E_F, we find a pair of spin-split surface states SS′ and SS″ crossing each other at the energy of -0.18 eV at $\overline{\Gamma}$. This is in agreement with the photoemission value of -0.34 eV at $\overline{\Gamma}$ [39,83]. A signature of these states can be detected in the normal emission spectra reported by Pletikosić *et al.* [81] and Elmers *el al.* [84] in the 0.2–0.3 eV interval below E_F

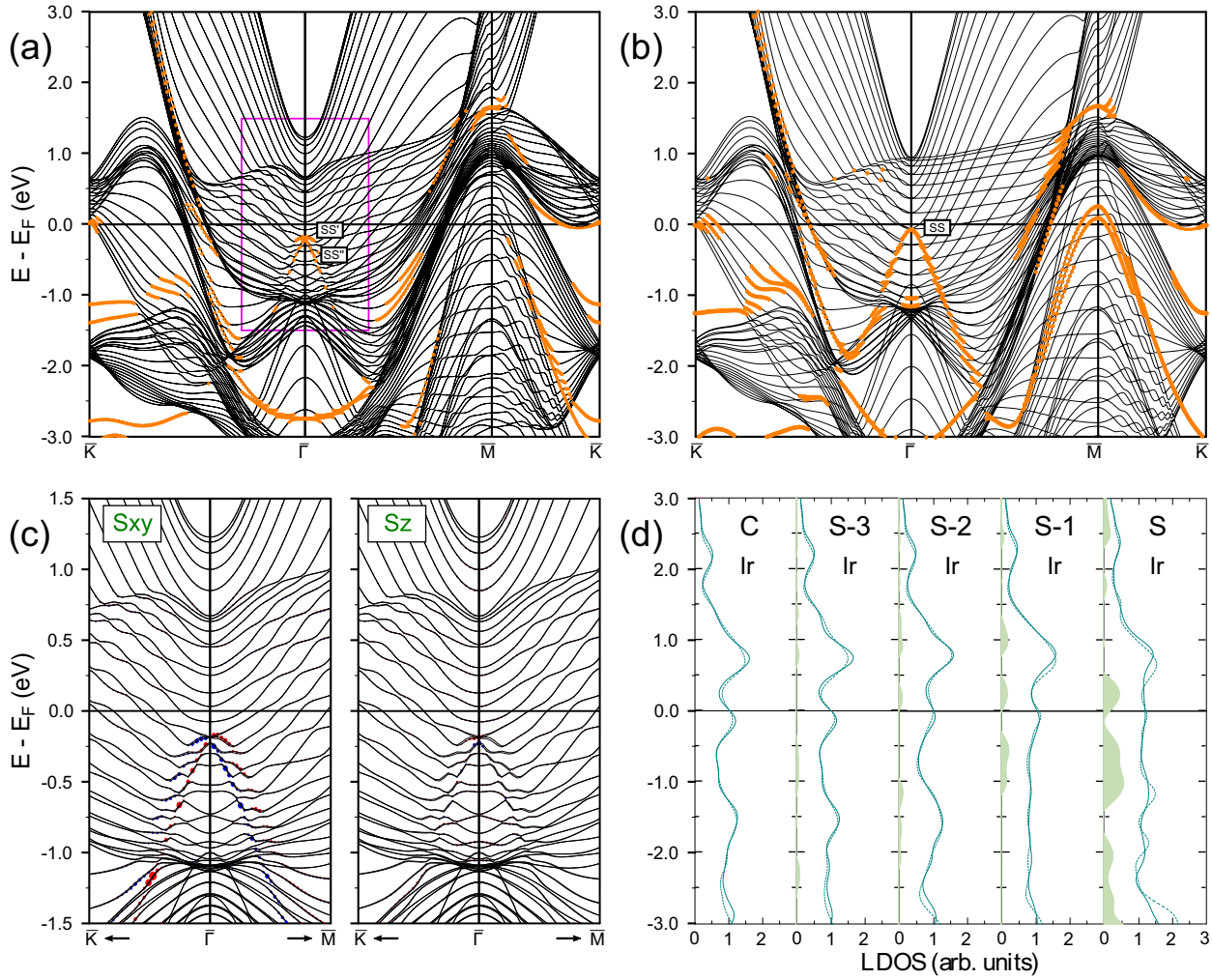

FIG. 1. Electronic structure of the Ir(111) surface calculated with (a) and without (b) spin-orbit interaction. The surface states and resonances are indicated by orange dots. The states discussed in the text are labeled by symbols. (c) magnifies the electronic structure inside the pink rectangular of (a) with a projection of spin on (left) the xy plane (S_{xy}) and (right) on the z axis (S_z). Red and blue colors indicate the opposite spin orientations. In (d), the layer density of states (LDOS) is shown for the top four [labeling of atomic layers starts from the surface (S) one] and the central (C) atomic layers. Solid (dashed) lines show LDOS obtained from the SOC (WSOC) calculation. Green regions show the excess of LDOS in a given layer in comparison with the bulk value.

as well. A downward dispersion of two resonance branches SS′ and SS″ follows a conventional Rashba-like shape despite the band splitting at the $\overline{\Gamma}$ point due to the finite-thickness effect. As seen in Fig. 1(b), in the Ir(111) electronic structure obtained without spin-orbit interaction this surface state pair merges into a doubly degenerate band denoted SS. Furthermore, without the inclusion of the spin-orbit interaction the SS band is shifted upward by about 0.11 eV and has a maximum at the energy of −0.07 eV.

At the $\overline{\Gamma}$ point, this surface state has a dominating s-p-orbital character as is evidenced by its charge density distribution reported in Fig. 2(a). However, its orbital composition rapidly transforms into a d type at finite wave vectors. In Figs. 2(b) and 2(c), we show the charge density plot for the upper SS′ and lower SS″ spin-split branches evaluated at $\mathbf{k}_\parallel = 0.04\overline{\Gamma M}$. Even at such small $\mathbf{k}_\parallel$ we observe the drastic transformation of the character of this surface state (especially the lower-energy SS″ one) into a d type. This is accompanied by more efficient penetration into the crystal. Upon the increase of the wave vector, this tendency is maintained for both branches.

In Fig. 1(c), we zoom the dispersion of these spin-split surface states showing its spin polarization, which demonstrates a typical Rashba-like spin texture. As seen in the left panel of Fig. 1(c), the in-plane xy spin polarization is significantly larger than the z spin component presented in the right panel. In our calculation, the Rashba splitting parameter α_R for this state is 1.1 eV Å. This value agrees rather well with the experimentally measured value of $\alpha_R \approx 1.3$ eV Å [39]. Our characteristics regarding this surface state are close to the calculated data for the 15- and 18-atomic-layer-thick slabs of Ir in Refs. [39] and [81], respectively.

Since the surface states SS′ and SS″ appear in the region where the bulk-band states exist, their dispersion has a typical resonance character. This is evidenced by the avoiding-crossing behavior involving bulk-like energy bands. Reaching the binding energy about 1.5 eV this surface state merges the bulk states in accord with the experiment [39,84].

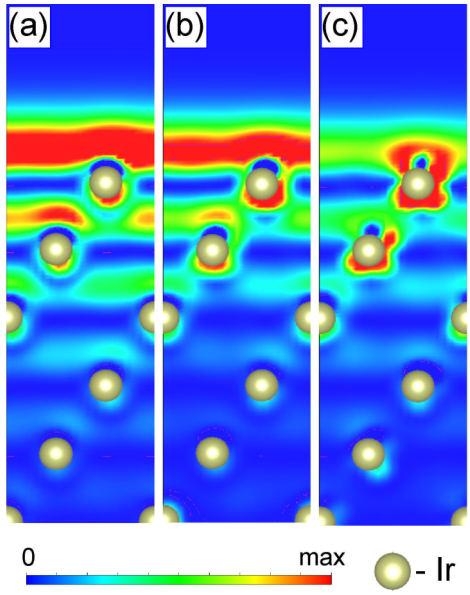

FIG. 2. (a) Charge density distribution of the SS' and SS'' states at the $\overline{\Gamma}$ point on the Ir(111) surface. (b) and (c) present it for these states at $\mathbf{k}_{\parallel} = 0.04\overline{\Gamma M}$, respectively. Grey dots show the Ir atomic positions.

In Fig. 1(a), below E_F one can find several other surface states at finite wave vectors. Some of them are true surface states owing to localization in the bulk energy gaps, like the spin-split ones with the energies of -1.12 and -1.38 eV at the $\overline{K}$ point. The other surface states disperse over a lower-energy gap with the energies of -2.76 and -3.09 eV at the $\overline{K}$ point. At wave vectors around the SBZ center, one can observe a surface state with the energy of -2.73 eV. It has a parabolic-like dispersion with the upward dispersion from the $\overline{\Gamma}$ point. Its clear surface character is ensured by its d type and location in a symmetry energy gap. A detailed description of properties of these and other surface states can be found in Ref. [79].

In Fig. 1(d), we present LDOS for the WSOC and SOC cases, as well as the difference between LDOS for four upper layers and LDOS of a central layer of the slab (which can be considered as representing a bulklike one). The surface states with dominating d-type character give rise to the strong peaks in LDOS at the surface. Especially a strong enhancement of the charge can be found in LDOS of the surface layer in the energy intervals between -1.4 and -0.2, -0.1 and 0.5, and below -1.7 eV. The effect of SOC in LDOS is significant and leads to the redistribution of all the features.

B. 1ML-Ir/Au(111)

In Figs. 3(a) and 3(b), we show the electronic structure of the 1ML-Ir/Au(111) system calculated, respectively, with and without SOC. The region delimited by a pink rectangular with addition of the spin texture is presented in Fig. 3(c) on the enhanced scale. We find that adsorption of the Ir ML produces a strong impact on the electronic structure of a pure Au(111) surface. First of all, we do not observe any signature of a Shockley s-p surface state in the wide energy gap around the SBZ center. Instead, in Fig. 3(a) we find six energy bands in the energy gap around the $\overline{\Gamma}$ point. Due to its spatial confinement to the Ir ML we interpret these states as the Ir-derived QWSs. At the $\overline{\Gamma}$ point we observe the energy gap in 0.30 eV between the bands $1'$-$1''$ and $2'$-$2''$. The energy gap between the bands $2'$-$2''$ and $3'$-$3''$ is 0.39 eV. The indirect gaps between the bands $1''$ and $2'$ is 0.20 eV, whereas that between the states $2''$ and $3'$ is 0.04 eV.

The most visible effect of the SOC inclusion is the spin splitting of all electronic states localized at the surface and a substantial energy shift of many of them. Moreover, the shape of these Ir-derived QWS bands changes notably. In particular, the bands $1'$ and $1''$ present a more parabolic-like behavior in the $\overline{\Gamma}$ point vicinity. At finite wave vectors, they are spin split. However, it is impossible to fit the dispersion of two resulting bands $1'$ and $1''$ using the Rashba model, since the energy splitting varies significantly with the wave vector. We relay such behavior to strong hybridization of these states with the QWSs 2 and 3 upon the switching on of the spin-orbit interaction. In the case of the 1ML Ir adlayer, this hybridization is notably stronger than in the 1ML-Pt/Au(111) case, where it is possible to describe the spin-orbit splitting of a similar band by a Rashba model with the splitting coefficient $\alpha_R = 1.5$ eV Å [54].

At the $\overline{\Gamma}$ point, the QWSs $1'$ and $1''$ coincide at the Rashba point with the energy of 0.5 eV. Its charge density distribution is reported in Fig. 4(a). Here the orbital composition of these states consists of dominating d orbital at Ir ions with a small portion localized in the vicinity of the top Au atomic layer. In both directions, the bands $1'$ and $1''$ disperse upward resembling the dispersion of the unoccupied s-p Ir bulk-like states of Fig. 1. As the wave vector shifts to $0.08\overline{\Gamma M}$, the s-p character in the density increases above the Ir ML as can be deduced from the charge density distribution of the states $1'$ and $1''$ reported in Figs. 4(b) and 4(c), respectively. When $\mathbf{k}_{\parallel}$ reaches to $0.16|\overline{\Gamma M}|$ this s-p mixture increases notably as shown in Figs. 4(d) and 4(e). The further from the $\overline{\Gamma}$ point, the stronger is the s-p contribution. Nevertheless, at any $\mathbf{k}_{\parallel}$ the d component is significant in these Ir-derived QWSs. Strong localization of this QWS in the Ir adlayer can be detected up to the energies about 2.5 eV.

The QWS bands $2'$ and $2''$ can be traced almost over a whole SBZ. Along the $\overline{\Gamma K}$ symmetry direction upon leaving the energy gap these states experience strong hybridization with the bulk-like states of the Au slab. It signals about its resonance nature in this region. At the wave vectors exceeding about $0.5\overline{\Gamma K}$, the corresponding resonance becomes to be occupied and loses its clear surface character. Upon its way toward the $\overline{K}$ point, it reappears again in the Au energy gap separating into two true surface states. Reaching the $\overline{K}$ point these states have the energies of -0.12 and -0.18 eV. On the contrary, along $\overline{\Gamma M}$ after living the energy gap the dispersion of the states $2'$ and $2''$ becomes almost the same. The resulting spin-degenerate band has a strong surface resonance character almost at any $k_{\parallel}$ in this symmetry direction. Only in the region close to E_F it experiences some hybridization with the gold bands and other Ir-derived QWS dispersing upward. After entering the Au energy gap in the vicinity of the $\overline{M}$ point it splits again in two separate branches. The resulting spin-resolved energy bands are at 1.24 and 1.42 eV at $\overline{M}$.

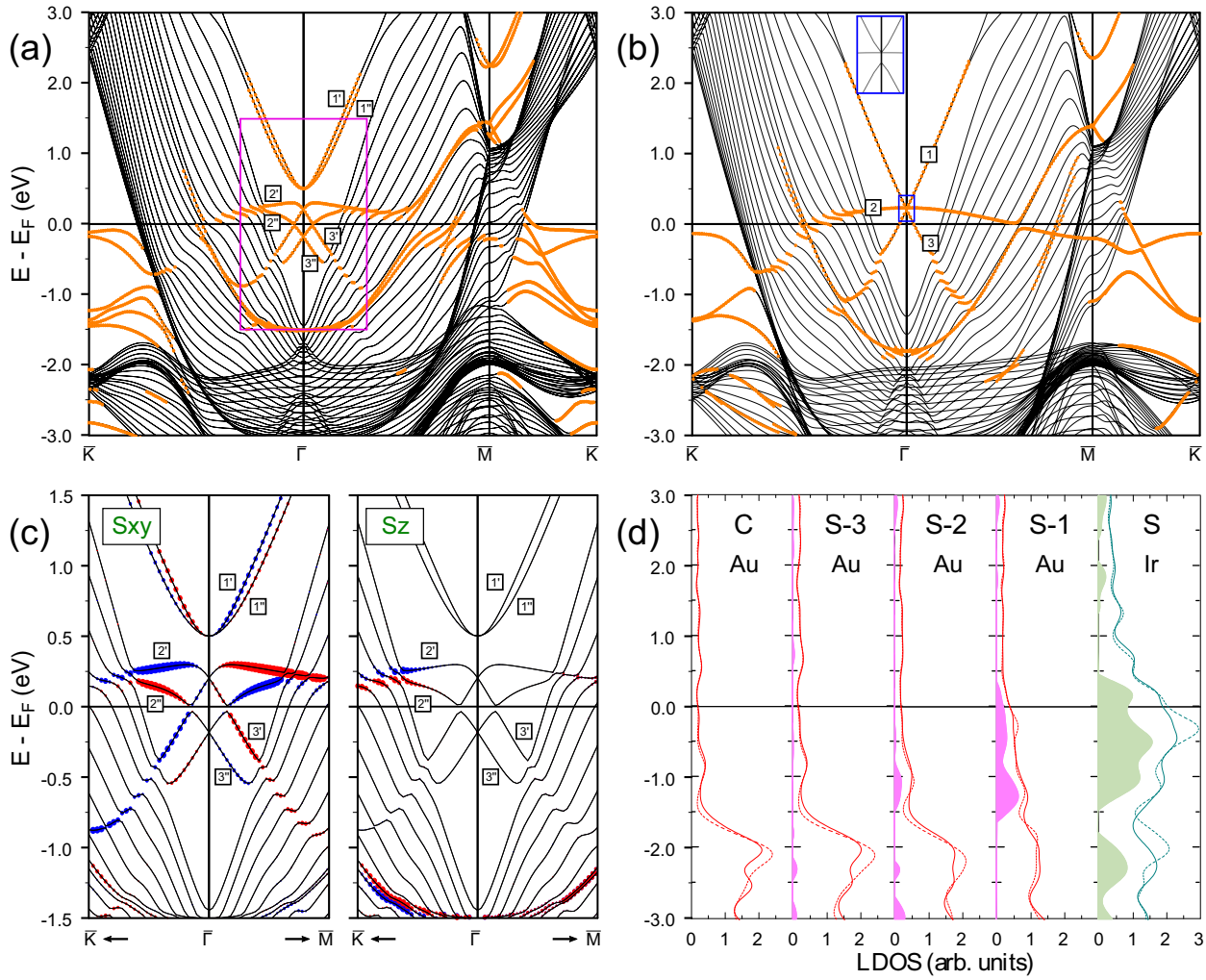

FIG. 3. Electronic structure of 1ML-Ir/Au(111) surface calculated with (a) and without (b) spin-orbit interaction. The quantum well states and resonances are indicated by orange dots. In (b), the insert magnifies the electronic structure inside the blue rectangular. The states discussed in the text are labeled by symbols. (c) magnifies the electronic structure inside the pink rectangular of (a) with a projection of spin on (left) the xy plane (S_{xy}) and (right) the z axis (S_z). Red and blue colors indicate the opposite spin orientations. In (d), the layer density of states (LDOS) is shown for the top four [labeling of atomic layers starts from the surface (S) one] and the central (C) atomic layers. Solid (dashed) lines show LDOS obtained from the SOC (WSOC) calculation. Green and pink regions show, respectively, the excess of LDOS in the Ir and Au layers in comparison with the bulk Ir and Au LDOS.

In the same energy gap, we find the other Ir spin-separated QWSs with the energy of 2.24 eV at $\overline{M}$. Due to its almost flat dispersion over a large portion of the SBZ, the bands $2'$ and $2''$ give a strong contribution to LDOS in the surface region around E_F. As is seen in Fig. 3(d), LDOS at the Ir atomic layer around E_F is almost two times larger than the Ir bulk value. Owing to the penetration of the wave function of the QWSs $2'$ and $2''$ into the Au substrate, LDOS at E_F in the top Au atomic layer is enhanced in comparison with the Au bulk interior by almost the same factor.

Figure 3(a) shows that the parts characterized by strong negative dispersion in the QWS bands $3'$ and $3''$ have a slope close to that observed in the surface state on a clean Ir(111) surface. These bands are completely occupied. The QWS $3'$ leaves the Au energy gap at the energies of ≈ -0.38 eV and becomes a strong resonance. Its dispersion can be traced up to the intersection with other Ir QWS having a parabolic-like positive dispersion. The latter QWS has bottom at $\overline{\Gamma}$ at energy of -1.5 eV and disperses up to about 1 eV above E_F in the $\overline{\Gamma K}$ direction. In the $\overline{\Gamma M}$ direction, it reaches the $\overline{M}$ point at energies below the Fermi level as a weak resonance. On the contrary, the QWS $3''$ exists in the Au energy gap only.

Other Ir-derived QWSs are observed in the Au energy gaps around the SBZ borders. Their properties resemble those of the Pt-induced QWSs in the 1ML-Pt/Au(111) system studied recently [54]. Therefore we do not discuss such states in this work.

In order to understand the evolution of the Ir-derived QWSs upon switching on the spin-orbit interaction, we investigated how the electronic structure of the 1ML-Ir/Au(111) system changes with varying the spin-orbit coupling coefficient α_{so}. The calculations were performed for $\alpha_{so} = 0.1$, 0.3, 0.5, 1.0, and 2.0. The resulting SOC electronic structure is shown in Fig. 5. In the panels (a)–(e), the dispersion of the states includes its spin projection in the xy plane. The size of the symbols is proportional to its projection magnitude. In the

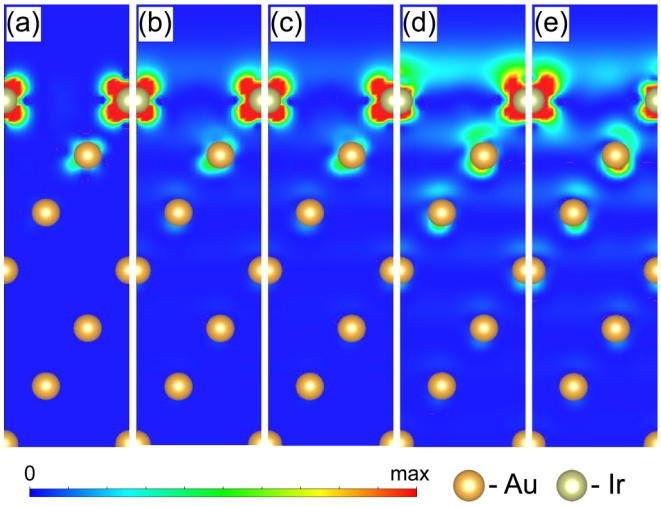

FIG. 4. (a) Charge density distribution of the QWSs $1'$ and $1''$ at the Dirac point in the 1ML-Ir/Au(111) system. (b) and (c) present it for these states at $\mathbf{k}_\parallel = 0.08\overline{\Gamma M}$, respectively. (d) and (e) show the same obtained at $\mathbf{k}_\parallel = 0.16\overline{\Gamma M}$. Yellow and grey dots show the Au and Ir atomic positions, respectively.

panels (f)–(j) the same band structure contains information about the z spin component of each state. One can see how the spin splitting of the energy bands with the localization at the Ir atomic layer gradually increases with the increasing the magnitude of α_{so}. At small α_{so}'s, the bands 1, 2, and 3 split into three separate groups without mixing between them at any α_{so}. At the smallest α_{so} value, the bands $2'$ and $2''$ in Figs. 5(a) and 5(f) have similar magnitude of the xy and z spin components at any finite $\mathbf{k}_\parallel$. In the case of $\alpha_{so} = 0.3$ the spin polarization of these states is mainly in the xy plane at $\mathbf{k}_\parallel$ in the vicinity of $\overline{\Gamma}$. At larger $k_\parallel$ the bands $2'$ and $2''$ have spin polarization predominantly in the z plane.

For $\alpha_{so} = 0.5$, the spin polarization of the bands $2'$ and $2''$ changes substantially. At finite $k_\parallel$ along $\overline{\Gamma K}$ the xy and z spin components are of the same size at the wave vectors in the Au(111) energy gap. Upon entering the region with the Au bulk-like energy bands the z spin orientation prevails. Along the $\overline{\Gamma M}$ direction the magnitudes of the xy and z spin components become similar upon approaching the energy gap border and maintain such ratio for larger $k_\parallel$.

When α_{so} reaches a value of 1.0 the spin texture of all the QWSs changes significantly. Along $\overline{\Gamma K}$ inside the Au energy gap the spin in the bands $2'$ and $2''$ orients mainly in the xy plane. Outside the gap the spin orientation in the z direction becomes dominating. As for the $\overline{\Gamma M}$ direction, the xy spin orientation is preferential at any $k_\parallel$.

Notice that the spin polarization of the QWS $2'$ and $2''$ with the variation of $\mathbf{k}_\parallel$ is different from a conventional Rashba-like shape exemplified in the case of the bands $1'$ and $1''$. Thus, the spin orientation of the bands $2'$ and $2''$ changes

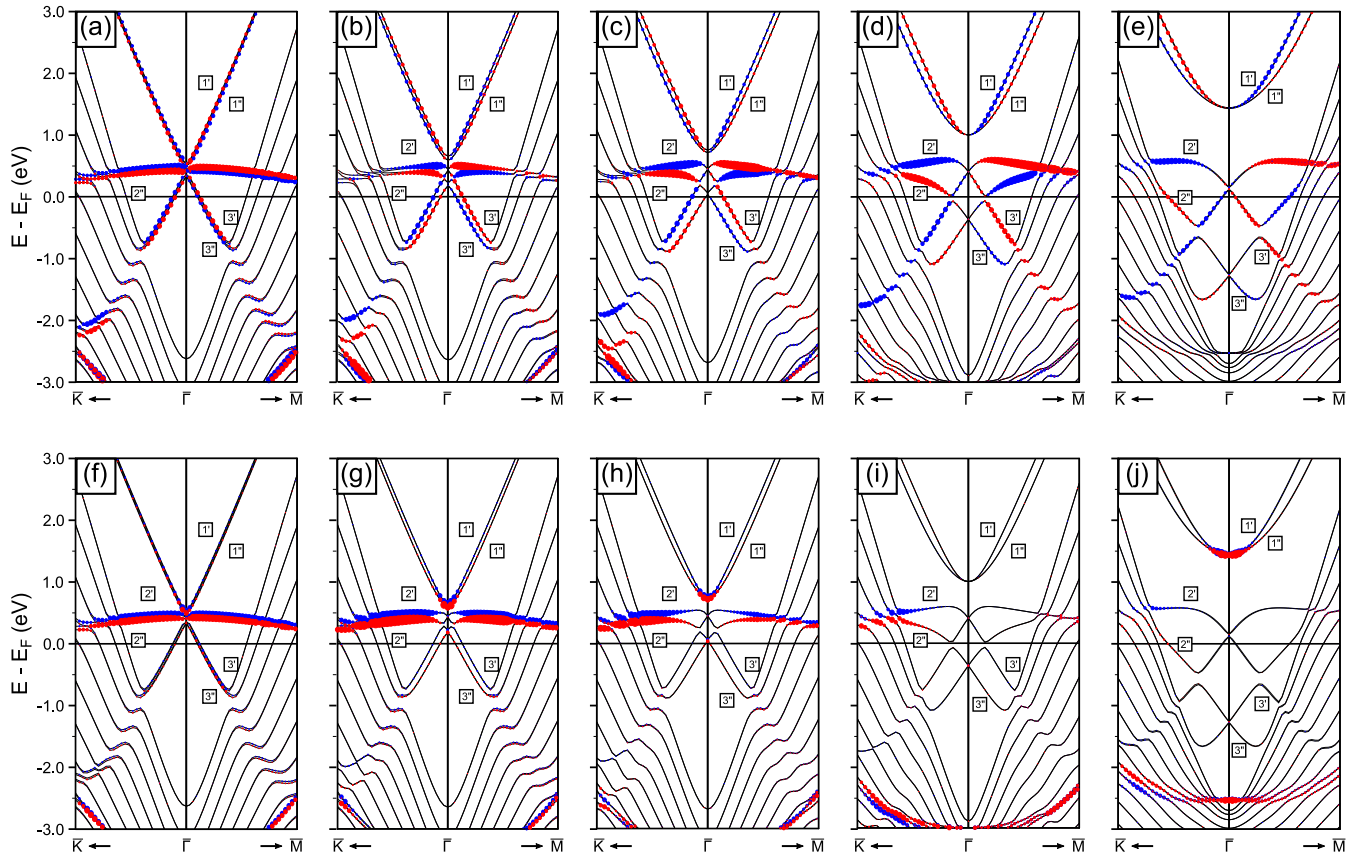

FIG. 5. Electronic structure of the 1ML-Ir/Au(111) surface calculated with the SOC coefficient α_{so} of (a) 0.1, (b) 0.3, (c) 0.5, (d) 1.0, and (e) 2.0 with a projection of spin on the xy plane (S_{xy}): blue (negative) and red (positive) dots. The same with α_{so} of (f) 0.1, (g) 0.3, (h) 0.5, (i) 1.0, and (j) 2.0 for the spin projection on the z axis (S_z): blue (negative) and red (positive) dots.

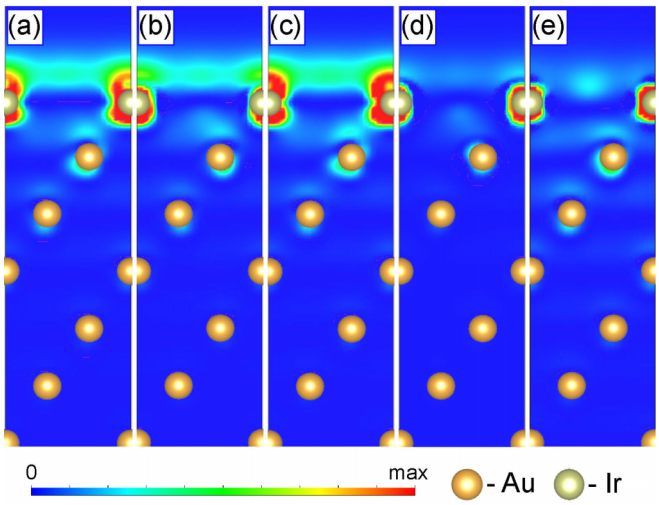

FIG. 6. (a) Charge density distribution of the QWSs 2′ and 2″ at the Dirac point in the 1ML-Ir/Au(111) system. (b) and (c) present it for these states at $\mathbf{k}_{\parallel} = 0.03\overline{\Gamma M}$, respectively. (d) and (e) show the same obtained at $\mathbf{k}_{\parallel} = 0.08\overline{\Gamma M}$. Yellow and grey dots show the Au and Ir atomic positions, respectively.

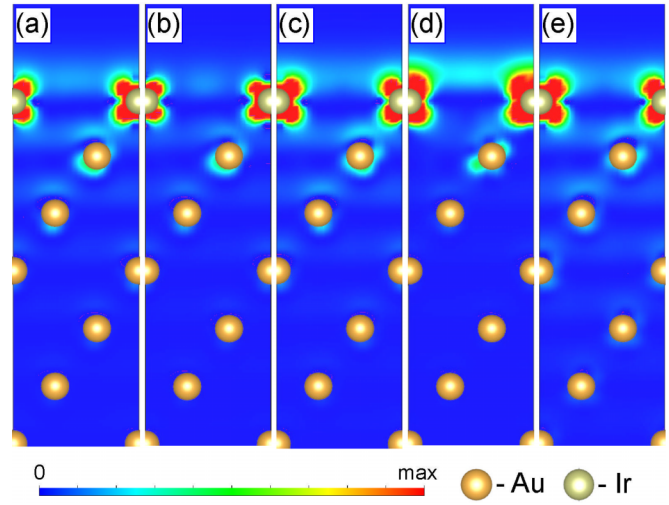

FIG. 7. (a) Charge density distribution of the QWSs 3′ and 3″ at the Dirac point in the 1ML-Ir/Au(111) system. (b) and (c) present it for these states at $\mathbf{k}_{\parallel} = 0.03\overline{\Gamma M}$, respectively. (d) and (e) show the same obtained at $\mathbf{k}_{\parallel} = 0.08\overline{\Gamma M}$. Yellow and grey dots show the Au and Ir atomic positions, respectively.

from positive (negative) to negative (positive) at finite $k_{\parallel}$'s along the same symmetry direction. This was observed in other systems [37] and can be explained in our case by the strong hybridization with the band 3′.

If we increase α_{so} up to 2.0 the spin texture of the 2′ and 2″ bands in Figs. 5(e) and 5(j) has a dominating xy polarization at all the wave vectors. The same, although at a lesser scale, is observed in the spin alignment of the QWS bands 1′ and 1″.

Regarding the transformation of the band 3 into a couple of the spin-split bands 3′ and 3″, its evolution with the α_{so} magnitude in Fig. 5 reveals that its spin texture is similar to that in a Rashba spin-split scenario at $\alpha = 0.1$, 0.3, and 0.5. These bands have the xy spin orientation at any $\mathbf{k}_{\parallel}$. This situation changes when the α_{so} value reaches 1.0 and 2.0. In these cases, the spin orientation of the 3′ band changes at finite $k_{\parallel}$'s. Again, we relay such spin-texture behavior in the band 3′ to its strong hybridization with the 2″ bands.

As seen in Fig. 3(c), between the bands 2″ and 3′ there is a small energy gap only. Strong hybridization between the QWSs 2′-2″ and 3′-3″ is evidenced in their spatial localization. In Fig. 6(a), we report charge density distribution for the states 2′ and 2″ at the $\overline{\Gamma}$ point. Here one can observe that in addition to the d-type contribution it has a strong admixture of the s-p character in the region above the Ir ML. Some portion of such symmetry can be found at the Ir-Au interface and between the top and the second Au atomic layers. When $\mathbf{k}_{\parallel}$ is at $0.03\overline{\Gamma M}$ the charge density of the 2′ and 2″ experiences notable transformation, as seen in Figs. 6(b) and 6(c). At such a small $k_{\parallel}$, the state 2′ loses its s-p contribution significantly and now the d admixture prevails. The same, although on a less scale is observed for the state 2″. Once we shift $\mathbf{k}_{\parallel}$ to $0.08\overline{\Gamma M}$ the charge density for the states 2′ and 2″ reported in Figs. 6(d) and 6(e), respectively, is almost completely dominated by the d-type contribution.

Variation in the charge density distribution of the QWSs 3′ and 3″ with the departure from the $\overline{\Gamma}$ point occurs as well, although on a lesser scale. Figure 7(a) confirms its essentially d character at the $\overline{\Gamma}$ point with only small s-p component above and under the Ir atomic layer position. At $0.03\overline{\Gamma M}$ the s-p-type contribution reduces in the QWS 2′ as is seen in Fig. 7(b). On the contrary, Fig. 7(c) shows that it remains almost the same in the QWS 2″. When $\mathbf{k}_{\parallel}$ changes to $0.08\overline{\Gamma M}$ the presence of the s-p admixture in the charge density of these states shown Figs. 7(d) and 7(e) becomes more evident.

In contrast to the bands 1′ and 1″, where the Rashba splitting model can not be applied, the spin splitting of the bands 2′-2″ and 3′-3″ is described by this model with certain limitations. The main problem is the bands 2′ and 2″, since it is not clear which sign of the effective mass is appropriate in this case. We take it negative considering the dispersion of the band 2 in the WSOC case of Fig. 3(b). Another problem consists in ambiguity in choosing a region in the $\mathbf{k}_{\parallel}$ space for the fitting procedure. In this work, we used two regions in the $\mathbf{k}_{\parallel}$ space for fitting. As reported in Table I, with fitting the dispersion of the bands 2′ and 2″ at $\mathbf{k}_{\parallel}$ close to the band 2′ maximum, we obtain $\alpha_R = 6.4$ eV Å. This value is probably

TABLE I. The fitted Rashba coefficient value (in eV Å) calculated for 1ML-Ir/Au(111) with the top position of the Ir monolayer, 1ML-Ir/Au(111) with the position of the Ir monolayer under the Au surface atomic layer, 2ML-Ir/Au(111), and 3ML-Ir/Au(111). The first line for each band set gives the values with fitting around the band extremum. The second line shows the values obtained from fitting the band dispersions around the Dirac point.

	1ML top	1ML under	2ML	3ML
bands 2′, 2″	6.4	5.9	5.0	2.8
	5.0	4.9	3.9	2.0
bands 3′, 3″	5.1	4.7	4.2	3.3
	3.3	3.5	3.4	2.4

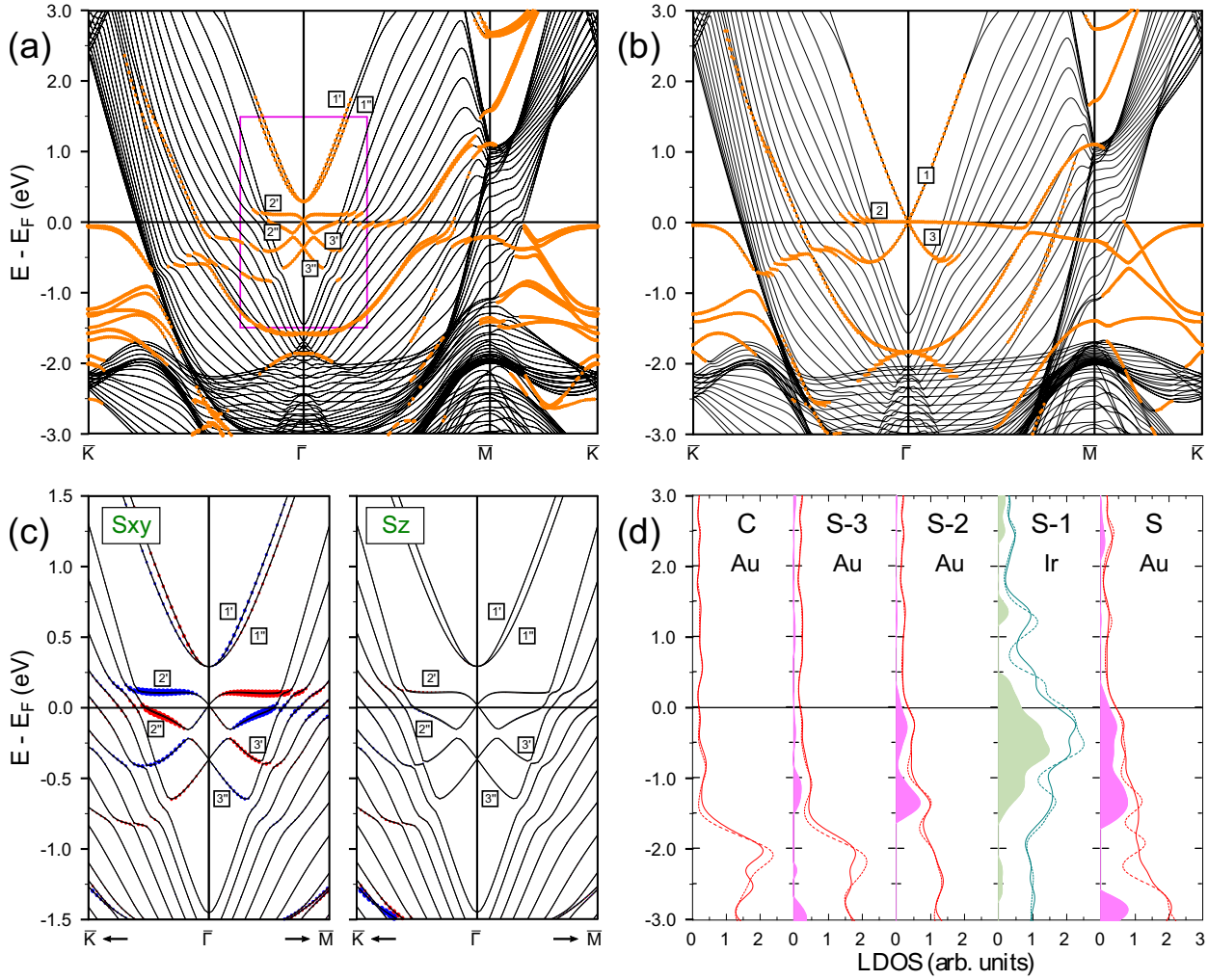

FIG. 8. Electronic structure of 1ML-Ir/Au(111) surface with the Ir monolayer placed under the top Au atomic layer calculated with (a) and without (b) spin-orbit interaction. The quantum well states and resonances are indicated by orange dots. The states discussed in the text are labeled by symbols. (c) magnifies the electronic structure inside the pink rectangular of (a) with a projection of spin on (left) the xy plane (S_{xy}) and on (right) the z axis (S_z). Red and blue colors indicate the opposite spin orientations. In (d), the layer density of states (LDOS) is shown for the top four [labeling of atomic layers starts from the surface (S) one] and the central (C) atomic layers. Solid (dashed) lines show LDOS obtained from the SOC (WSOC) calculation. Green and pink regions show, respectively, the excess of LDOS in the Ir and Au layers in comparison with the bulk Ir and Au LDOS.

the largest spin-splitting coefficient reported up to now in metallic systems. In the case of fitting the dispersion of the bands $2'$ and $2''$ in a region close to the Rashba point we obtain $\alpha_R = 5.0$ eV Å which is rather large as well. Notice that in the case of the Pt ML adsorption studied in Ref. [54] such a procedure could not be applied for the description of the spin splitting of the similar QWSs.

Regarding the spin splitting in the bands $3'$ and $3''$, the fitting procedure again is rather ambiguous. If we take as a reference the regions of $k_\parallel$ close to the maximum in the band $3'$ dispersion, the fitting gives $\alpha_R = 5.1$ eV Å. Choosing the $\overline{\Gamma}$-point vicinity results in $\alpha_R = 3.3$ eV Å.

In order to address the Au segregation effect in the 1ML-Ir/Au(111) system, in this work, we investigated the case when an Ir ML is situated under the Au surface atomic layer. Figure 8 demonstrates the band structure of such a system calculated with (a) and without (b) SOC. By comparing these two panels we conclude that the switching on the spin-orbit interaction produces a similar effect as in the previously discussed system.

Comparison of the SOC band structure presented in Fig. 8(a) with that in Fig. 3(a) reveals that the variation in the Ir ML position with respect to the Au surface atomic layer produces relatively little effect on the energy position and dispersion on the Ir-induced QWSs. We relay such insensitivity of the Ir-derived electronic states to its predominantly d character. Nevertheless, some modifications can be appreciated. As for the QWSs $1'$-$1''$, $2'$-$2''$, and $3'$-$3''$ of primary interest here, their energy positions in the Au energy gap experience downward shift by about 0.2 eV. The shape of the bands $1'$ and $1''$ is hardly affected by the variation in the Ir ML position. On the contrary, the downward shift of the band $2'$ depends slightly on the wave-vector magnitude being maximal at the SBZ center. As a result, its dispersion in the Au energy gap becomes almost flat and appears closer to E_F crossing the corresponding Rashba point. As for the bands $3'$ and $3''$ its

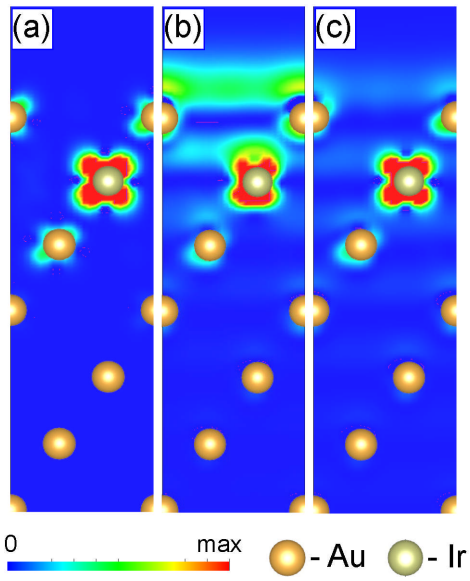

FIG. 9. (a) Charge density distribution at the Dirac point of the Ir-derived QWSs (a) $1'$ and $1''$, (b) $2'$ and $2''$, and (c) $3'$ and $3''$ in 1ML-Ir/Au(111) with vertical position of the Ir monolayer under the top Au atomic layer. Yellow and grey dots show the Au and Ir atomic positions, respectively.

dispersion is also affected by such downward shift. In the $\overline{\Gamma K}$ direction, the bands $3'$ and $3''$ disperse down to energy of -0.35 and about -0.6 eV, respectively. After reaching the bottom the dispersion of corresponding resonances becomes positive. After crossing with another resonance state its dispersion changes the sign again. Entering the Au energy gap around the $\overline{K}$ point these QWSs reestablish its true surface character with very close dispersion and almost reaches E_F at $\overline{K}$. On the contrary, along the $\overline{\Gamma M}$ direction the QWS bands $3'$ and $3''$ disappear rather quickly upon entering the Au bulk-band continuum.

Some other changes can be noted in the dispersion of the other Ir-derived states. For instance, the lowest-energy Ir QWSs in the upper-energy gat at $\overline{K}$ shift upward and locate in the Au energy gap increasing its localization in the Ir ML.

The spin texture of the QWS bands $1'$-$1''$, $2'$-$2''$, and $3'$-$3''$ shown in Fig. 8(c) resembles that in Fig. 3(c) although a small reduction in the xy spin amplitude in the QWS reported on the left panel of Fig. 8(c) can be noted. As for the z spin orientation, the right panel of Fig. 8(c) confirms that it is negligible for all the states above -1 eV. The fitted values for the Rashba splitting coefficients for the QWSs 1, 2, and 3 can be found in Table I. Some reduction of the α_R can be noted in comparison to the Ir top position. Nevertheless, the unusually large values are obtained even in this case despite local symmetry in the Ir ML vicinity in the z direction and essentially d character of the Ir QWSs. This can be explained by the role played by the s-p component in these states, which is larger expanded in the space as seen in Fig. 9 and can feel the different environment around the Au top atomic layer in comparison to the gold interior.

Regarding LDOS reported in Fig. 8(d), its comparison with the case when the 1ML Ir atomic layer is placed on top of the Au(111) surface reveals a few quantitative differences but qualitatively its behavior is similar. Spin polarization for this case also very close to the previous one. Thus we may conclude that all features of this heterostructure are not very sensitive to the position of the Ir adlayer with respect to the top Au atomic layer.

C. 2ML-Ir/Au(111)

The calculated electronic structure of the 2ML-Ir/Au(111) system is presented in Fig. 10. In the SOC band structure of Fig. 10(a), one can see that the addition of an Ir ML produces numerous modifications in the electronic states in the surface region. For instance, the number of the Ir-derived QWS bands increases in the Au energy gaps at the SBZ borders and its energy positions are different from those in Fig. 3(a). In particular, four unoccupied spin-resolved QWS bands appear in the vicinity of the $\overline{MK}$ line. Such an increase of the QWS number and energy variation is in accord with the increased thickness of the Ir film. The number of Ir-derived QWS pairs in the Au energy gap around the SBZ center increases from three to four as well.

The dispersion of the bands $1'$ and $1''$ resembles that in the case of 1ML-Ir/Au(111), although its parabolic shape in the vicinity of $\overline{\Gamma}$ in Fig. 10(a) is more pronounced. Similar to the WSOC case of Fig. 10(b) these bands are degenerate at the $\overline{\Gamma}$ point. However, like in the 1ML-Ir/Au(111) case, the value of spin splitting of the QWSs $1'$ and $1''$ depends on the wave vector magnitude. As a result, we could not fit their dispersion by the Rashba model in a satisfactory way. The spin texture of the QWSs $1'$ and $1''$ reported in Fig. 10(d) presents strong z spin component in the $\overline{\Gamma}$-point vicinity, whereas the in-plane component is negligible. Upon increase of the wave vector, the spin alinement becomes in-plane-like, similar to a typical Rashba-like in-plane spin texture.

Due to SOC, the energy gap in 0.39 eV exists between the QWSs $1'$-$1''$ and $2'$-$2''$ at the $\overline{\Gamma}$ point. The minimal indirect gap between the QWSs $1''$ and $2'$ is of 0.15 eV. The dispersion of the QWS $2'$ is positive at any $\mathbf{k}_\parallel$ in Fig. 10(a). Along the $\overline{\Gamma K}$ symmetry direction this QWS reaches the Au energy gap border at the energy about 0.65 eV merging the QWS $2''$. Interaction with the Au bulk-like states of the resulting resonance is so strong that it disappears very quickly. Along the $\overline{\Gamma M}$ direction, the dispersion of the QWSs $2'$ and $2''$ becomes the same after leaving the Au energy gap. It can be traced over the large distance since after entering the Au projected-bulk-state continuum it maintains its strong surface state character. It disappears in the vicinity of the $\overline{M}$ point only.

Comparing Figs. 10(a) and 10(b), one can see that the SOC switching on results in a strong spin-orbit splitting of the doubly degenerate QWS 2 in the Au energy gap. The resulting QWSs $2'$ and $2''$ experience also notable downward shift at the SBZ center. Interestingly, the spin splitting of the QWS 2 is notably larger than the similar Pt-derived QWS in the 2ML-Pt/Au(111) system [54]. Moreover, the shape of the $2'$ and $2''$ QWS bands in 2ML-Ir/Au(111) allows us to apply the Rashba model. The values of the Rashba coefficient are reported in Table I. The values for the QWSs $2'$ and $2''$ are somewhat lower than in the 1ML-Ir/Au(111) case but still

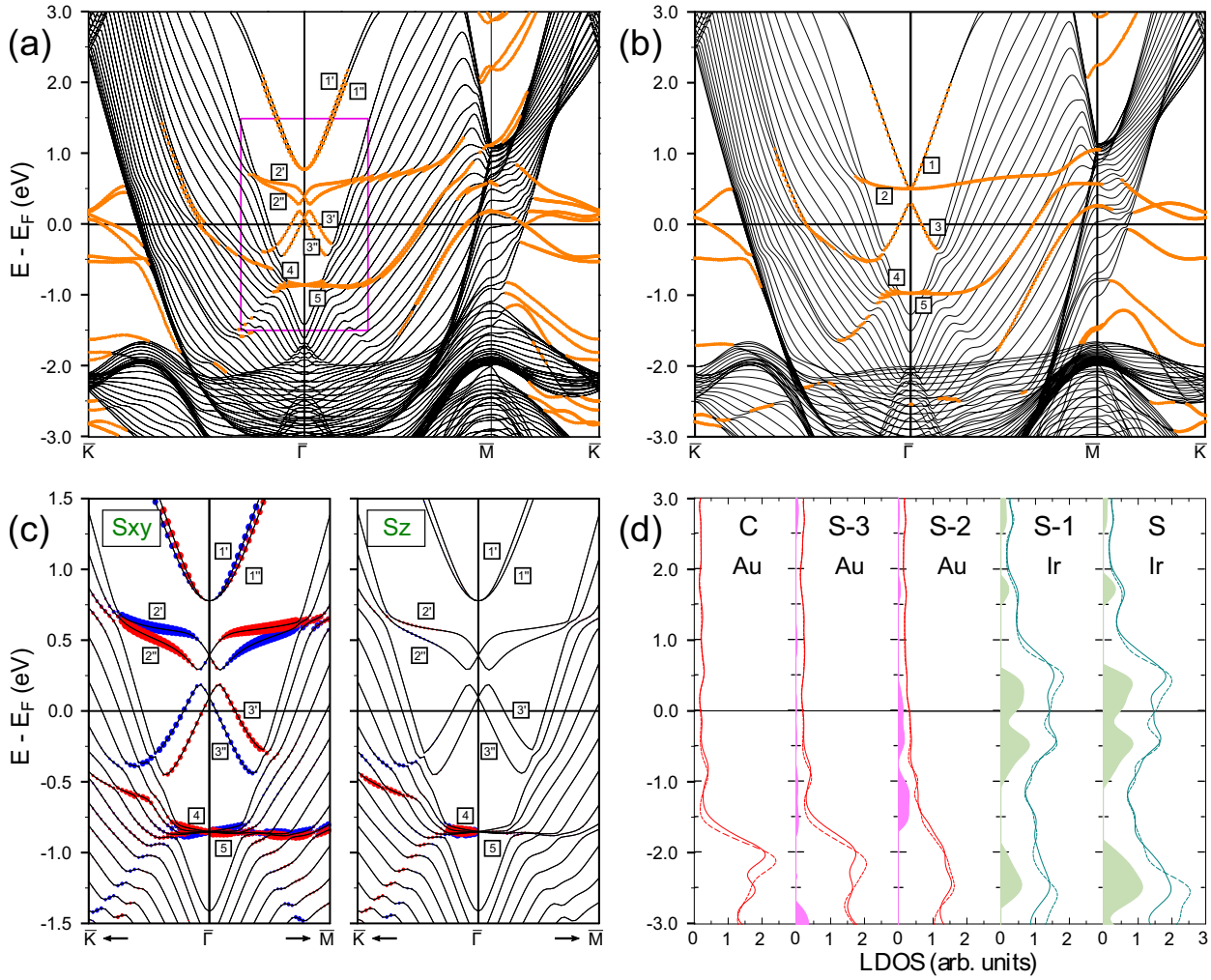

FIG. 10. Electronic structure of 2ML-Ir/Au(111) surface calculated with (a) and without (b) spin-orbit interaction. The quantum well states and resonances are indicated by orange dots. The states discussed in the text are labeled by symbols. (d) magnifies the electronic structure inside the pink rectangular of (a) with a projection of spin on (left) the xy plane (S_{xy}) and on (right) the z axis (S_z). Red and blue colors indicate the opposite spin orientations. In (d), the layer density of states (LDOS) is shown for the top four [labeling of atomic layers starts from the surface (S) one] and the central (C) atomic layers. Solid (dashed) lines show LDOS obtained from the SOC (WSOC) calculation. Green and pink regions show, respectively, the excess of LDOS in the Ir and Au layers in comparison with the bulk Ir and Au LDOS.

are unusually large. Strong hybridization of these QWSs with other Ir QWSs in the vicinity of the SBZ center is reflected in their spin texture reported in Fig. 10(c). There one can see that the in-plane spin orientation of QWSs $2'$ and $2''$ changes the sign on each side from the Rashba point which is not described by the Rashba model.

In Fig. 10(a), beyond the Rashba point vicinity, the QWSs $3'$ and $3''$ have strong downward dispersion upon increasing the wave vector. In the $\overline{\Gamma K}$ direction, upon reaching the Au band-gap boundary the QWS $3'$ transforms into a strong resonance with a minimum at the energy of -0.38 eV. At larger $k_\parallel$ its dispersion can be hardly traced due to strong hybridization with other Ir QWS. On the contrary, the QWS $3''$ disappears rather quickly after leaving the energy gap. The same we observe for both these QWSs in the $\overline{\Gamma M}$ direction.

The dispersion of the spin-split QWSs $3'$ and $3''$ is modified significantly in comparison with the "parent" QWS 3. At the $\overline{\Gamma}$ point the energy position of the Rashba point of these bands locates at significantly lower energy shifting to 0.10 eV. Its dispersion shape and spin-texture reported in Fig. 10(c), is closer to the conventional Rashba model. This is also reflected in the smaller difference between the Rashba coefficients obtained in the two fitting procedures as evidenced from Table I.

An increased number of the Ir MLs results in the addition of two other Ir-derived spin-degenerate QWSs at lower energies in the Au energy gap around the SBZ center. In Figs. 10(a) and 10(b), these states are labeled as 4 and 5. They are degenerate at $\overline{\Gamma}$ at -0.85 eV. A similar set of doubly degenerate QWSs is observed in the 2ML-Pt/Au(111) system at the bottom of the Au energy gap [54]. However, SOC does not separate the QWSs 4 and 5 at the SBZ center in 2ML-Ir/Au(111) like it occurs in 2ML-Pt/Au(111) [54]. In the vicinity of $\overline{\Gamma}$ the dispersion of the QWS 4 band is almost flat in both symmetry directions. It disappears beyond the energy gap. However, along the $\overline{\Gamma K}$ it reappears again at larger wave vectors and energies as a strong resonance with positive

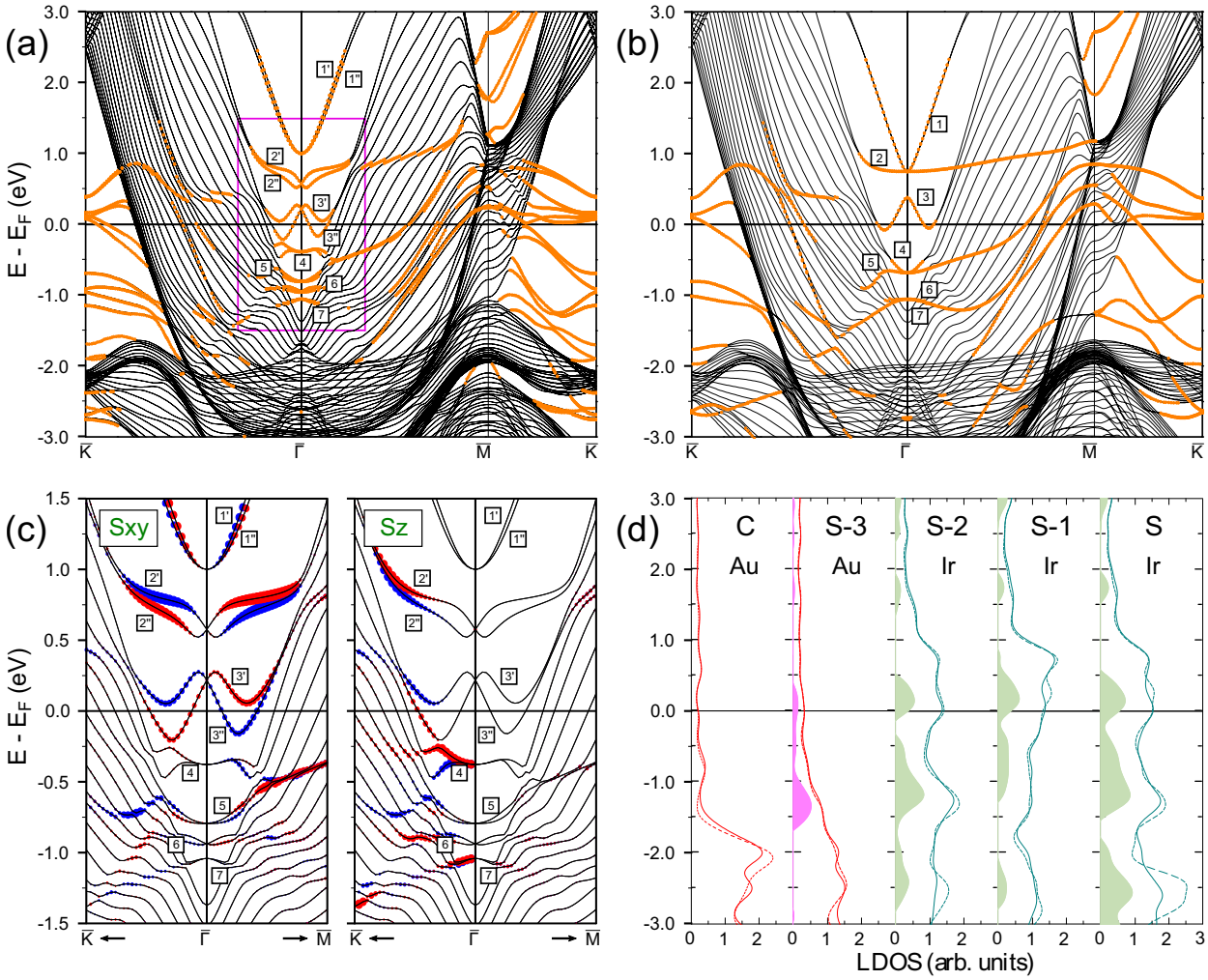

FIG. 11. The electronic structure of 3ML-Ir/Au(111) surface calculated with (a) and without (b) spin-orbit interaction. The quantum well states and resonances are indicated by orange dots. The states discussed in the text are labeled by symbols. (d) magnifies the electronic structure inside the pink rectangular of (b) with a projection of spin on (left) the xy plane (S_{xy}) and on (right)the z axis (S_z). Red and blue colors indicate the opposite spin orientations. In (d), the layer density of states (LDOS) is shown for the top four [labeling of atomic layers starts from the surface (S) one] and the central (C) atomic layers. Solid (dashed) lines show LDOS obtained from the SOC (WSOC) calculation. Green and pink regions show, respectively, the excess of LDOS in the Ir and Au layers in comparison with the bulk Ir and Au LDOS.

dispersion that can be detected up to the energy of about 1.5 eV above E_F.

Being flat inside the energy gap the QWS 5 band dispersion almost coincides with that of the QWS 4. In the $\overline{\Gamma K}$ direction, the QWS 5 state after reaching the energy gap border splits into two spin-resolved resonances with negative dispersion. In Fig. 10(a), its presence can be observed down to the energy of -1.7 eV. A much more weak resonance linked to the QWSs 4 and 5 with a similar downward dispersion can be detected in $\overline{\Gamma M}$ as well. In the $\overline{\Gamma M}$ the QWS 5 maintains almost the same energy over about $1/3|\overline{\Gamma M}|$. At larger wave vectors it disperses upward, crosses E_F, and reaches the $\overline{M}$ point vicinity where it ceases to exist.

At the SBZ borders, all other Ir QWSs experience notable spin-orbit splitting as well. The splitting depends strongly on the wave vector. Therefore it is difficult to apply a Rashba model for the description of these states.

The presence of the QWSs with strong localization in the Ir adlayer produces significant increase in LDOS of both Ir MLs as seen in Fig. 10(d). In particular, a strong increase is observed in the energy interval from -1.1 to 0.6 eV. Even a larger LDOS increase can be found in the surface Ir atomic layer at energies around -2.5 eV. In the interface Au atomic layer, we also observe some enhancement of LDOS around E_F and in the -0.9 to -1.7 eV energy interval.

D. 3ML-Ir/Au(111)

In Figs. 11(a) and 11(b), the SOC and WSOC band structure of the 3ML-Ir/Au(111) system is presented, respectively. Their comparison demonstrates that in the 3ML-Ir/Au(111) system the inclusion of SOC produces a notable impact on the Ir-derived QWSs. In particular, as in the previously discussed systems, the energy position and dispersion of the QWSs change significantly. Nevertheless, the spin splitting is reduced in all the QWSs in accord with the increased thickness of the Ir adlayer. The QWSs $1'$-$1''$, $2'$-$2''$, and $3'$-$3''$ can be found at somewhat higher energies than in the systems

containing the thinner Ir adlayers. Their dispersion is rather close to the 2ML-Ir/Au(111) case. The upper-energy QWSs $1'$ and $1''$ have an upward parabolic-like dispersion with a clear surface-like character up to energies about 2.5 eV. These bands have the bottom at 1.0 eV and are spin-split at finite wave vectors. However, such a splitting is notably smaller than in Figs. 3(a) and 10(a). Again, the Rashba model can not be applied for the description of the spin splitting of these states in 3ML-Ir/Au(111).

The QWSs $2'$ and $2''$ have a much flatter dispersion. Inside the Au energy gap the spin splitting of the QWSs $2'$ and $2''$ in Fig. 11(a) is re duced notably as well. This is confirmed by the fitted Rashba coefficients reported in Table I, which drop significantly in comparison with the previously discussed three systems. Their energy at the Rashba point is 0.58 eV and the separation caused by SOC diminishes upon approaching the energy gap boundaries in both symmetry directions. In the $\overline{\Gamma K}$ direction, the QWSs $2'$ and $2''$ evolve in the Au energy gap up to the energy about 1.1 eV. Having reached the gap boundary these bands transform into resonance and quickly lose their surface character inside the Au bulk-band continuum. Along $\overline{\Gamma M}$ these QWSs are degenerate beyond the gold energy gap and have a resonance character with positive dispersion. Interestingly, even at a such Ir film thickness, the Ir-derived QWSs feel rather efficiently the details of the substrate band structure.

Like in 2ML-Ir/Au(111), in Fig. 11(a), we find the Ir generated QWSs $3'$ and $3''$ in the vicinity of E_F. The Rashba point of these states is at 0.22 eV. As seen in Fig. 11(a), these QWSs exist only inside the energy gap. In both symmetry directions, these QWSs have one minimum and one maximum. Such dispersion shape ensures that the lower-energy band $3''$ crosses E_F only. Besides the strong deviation of the dispersion of these QWSs from a parabolic-like shape, its spin texture in Fig. 11(c) has essentially a conventional in-plane alignment. Nevertheless, at finite wave vectors along $\overline{\Gamma K}$, a nonzero z spin component in these QWSs can be detected. The Rashba coefficients for these states is reduced significantly in comparison to the other systems.

In the occupied part of the band structure of Fig. 11(a), we find other four Ir-induced QWSs denoted as 4, 5, 6, and 7, which are spin-degenerate at the $\overline{\Gamma}$ point. As Figs. 11(a) and 11(c) evidence, SOC produces strong energy separation of the upper-energy QWSs 4 and 5. Thus, at $\overline{\Gamma}$, an energy gap of 0.42 eV opens between them. On the contrary, the spin-orbit splitting of the QWSs 4 and 5 is rather modest. Only at $\mathbf{k}_\parallel$ in the vicinity of $0.3\overline{\Gamma K}$ large energy separation in the pair originated from the QWS 4 is observed. It is caused by strong hybridization with the QWS $3''$. We relay to this hybridization the notable z spin component in these QWSs observed in Fig. 11(c) along $\overline{\Gamma K}$. Beyond the $\overline{\Gamma}$ point, the upper QWS 4 disperses upwards and splits into two branches by SOC. At larger wave vectors its dispersion becomes negative. Upon approaching the gap boundaries on both sides from the SBZ center, it transforms into a weak resonance. After that, it is difficult to follow its dispersion.

The lower-energy QWS 5 splits into two spin-resolved bands at finite wave vectors with a positive dispersion and a large effective mass around the SBZ center. After reaching the gap boundary in the $\overline{\Gamma K}$ direction, its dispersion becomes negative. It has a minimum at about -0.73 eV. At larger wave vectors this state loses its surface character. In contrast, along the $\overline{\Gamma M}$ direction, after entering the Au-projected-bulk-state continuum the QWS 5 presents pronounced positive dispersion and reaches the maximum at 0.84 eV in the vicinity of the $\overline{M}$ point.

The presence of two other Ir QWSs labeled as 6 and 7 at the bottom of the substrate energy gap around the SBZ center in contrast with a single QWS 6 in 3ML-Pt/Au(111) outside the Au band gap [54] is explained by the upper energy position of the valence d bands in Ir. In the 3ML-Ir/Au(111) SOC band structure, we find that an energy gap of 0.10 eV opens between the QWSs 6 and 7. However, the spin-orbit splitting of the QWSs 6 and 7 is small. Only upon the transformation into resonance states after leaving the energy gap, the energy separation between the spin-split bands becomes notable. However, it is difficult to analyze its dispersion in terms of the Rashba model due to strong hybridization effects.

Other QWSs with true surface and a resonance surface character can be observed at finite wave vectors in Fig. 11(a). The properties of the majority of them are very similar to those discussed in 3ML-Pt/Au(111) [54]. Therefore we do not concentrate on them in this publication.

Figure 11(d) demonstrates that the quantization of the Ir electronic states in 3ML-Ir/Au(111) produces a strong enhancement in LDOS in four upper atomic layers. Strong peaks in the vicinity of E_F with the maximum at 0.2 eV are observed in all three Ir atomic layers. In the occupied part, the enhancement of charge in LDOS is maximal in the surface Ir layer. Interestingly, in the interface Ir layer, LDOS below E_F is notably larger than in the second layer. In the interface Au atomic layer LDOS is enhanced as well in certain energy regions. Especially the large increase we observe in the energy region between -0.8 and -1.7 eV.

IV. CONCLUSIONS

We have performed the density-functional-theory calculations of the electronic structure of the nML-Ir/Au(111) heterostructures with $n = 1$, 2, and 3. Varying the adlayer thickness allowed us to study the formation of the Ir-derived valence quantum-well states in a systematic way with special attention to the states in a wide s-p energy gap of the Au(111) substrate at the surface Brillouin zone center. In order to address the impact of spin-orbit interaction in such systems, the calculations with and without the spin-orbit coupling were performed.

We find that the spin-orbit splitting of the Ir quantum-well states is very large in nML-Ir/Au(111) at all the considered n. In particular, the maximal value of the Rashba coefficient $\alpha_R = 6.4$ eV Å was obtained for one QWS in 1ML-Ir/Au(111). Moreover, for the upper-energy QWSs in the vicinity of the SBZ center in all the systems the values for α_R exceeding 2 eV Å were obtained. We relay such strong spin-orbit splitting in the Ir-derived QWSs to its dominating d character and strong mutual hybridization.

A large number of strongly localized at the surface quantum well states results in a strong enhancement of the layered density of states at energies around the Fermi level in comparison to the clean Ir(111) and Au(111) surfaces. Energy

positions of the QWSs according to the Fermi level strongly depend on the Ir adlayer thickness which may be attractive for the engineering of such electronic systems. We expect that such a system would be interesting for the observation of the effects found in this study.

ACKNOWLEDGMENTS

I.V.S. acknowledges the Ministry of Science and Higher Education of the Russian Federation for funding in framework of State Task (No. 0721-2020-0033). Y.M.K. acknowledges the Fundamental Research Program of the State Academies of Sciences, line of research III.23.2.9 and the Tomsk State University competitiveness improvement program (Project No. 8.1.01.2018). V.M.S. acknowledges funding from the Project of the Basque Government (Q-NANOFOT IT1164-19). E.V.C. acknowledges the Saint-Petersburg State University (Project No. 51126254). V.M.S. and E.V.C. acknowledge the Spanish Ministry of Economy, Industry and Competitiveness MINEICO (Projects Nos. FIS2016-76617-P and FIS2016-75862-P).

Calculations were performed using computational resources provided by Resource Center "Computer Center of SPbU" and the SKIF-Cyberia supercomputer at the National Research Tomsk State University.

[1] G. Dresselhaus, Phys. Rev. **100**, 580 (1955).
[2] E. I. Rashba, Sov. Phys. Solid State **2**, 1109 (1960).
[3] A. Manchon, H. C. Koo, J. Nitta, S. M. Frolov, and R. A. Duine, Nat. Mater. **14**, 871 (2015).
[4] A. Soumyanarayanan, N. Reyren, A. Fert, and C. Panagopoulos, Nature (London) **539**, 509 (2016).
[5] E. E. Krasovskii, J. Phys. Condensed Matter **27**, 493001 (2015).
[6] Y. A. Bychkov and E. I. Rashba, JETP Lett. **39**, 78 (1984).
[7] Y. A. Bychkov and E. I. Rashba, J. Phys. C: Solid State Phys. **17**, 6039 (1984).
[8] S. LaShell, B. A. McDougall, and E. Jensen, Phys. Rev. Lett. **77**, 3419 (1996).
[9] G. Nicolay, F. Reinert, S. Hüfner, and P. Blaha, Phys. Rev. B **65**, 033407 (2001).
[10] J. Henk, A. Ernst, and P. Bruno, Phys. Rev. B **68**, 165416 (2003).
[11] Y. M. Koroteev, G. Bihlmayer, J. E. Gayone, E. V. Chulkov, S. Blügel, P. M. Echenique, and P. Hofmann, Phys. Rev. Lett. **93**, 046403 (2004).
[12] J. I. Pascual, G. Bihlmayer, Y. M. Koroteev, H.-P. Rust, G. Ceballos, M. Hansmann, K. Horn, E. V. Chulkov, S. Blügel, P. M. Echenique, and P. Hofmann, Phys. Rev. Lett. **93**, 196802 (2004).
[13] I. Gierz, T. Suzuki, E. Frantzeskakis, S. Pons, S. Ostanin, A. Ernst, J. Henk, M. Grioni, K. Kern, and C. R. Ast, Phys. Rev. Lett. **103**, 046803 (2009).
[14] S. Yaginuma, K. Nagaoka, T. Nagao, G. Bihlmayer, Y. M. Koroteev, E. V. Chulkov, and T. Nakayama, J. Phys. Soc. Jap. **77**, 014701 (2008).
[15] C. R. Ast, J. Henk, A. Ernst, L. Moreschini, M. C. Falub, D. Pacilé, P. Bruno, K. Kern, and M. Grioni, Phys. Rev. Lett. **98**, 186807 (2007).
[16] G. Bihlmayer, S. Blügel, and E. V. Chulkov, Phys. Rev. B **75**, 195414 (2007).
[17] S. Mathias, A. Ruffing, F. Deicke, M. Wiesenmayer, I. Sakar, G. Bihlmayer, E. V. Chulkov, Y. M. Koroteev, P. M. Echenique, M. Bauer, and M. Aeschlimann, Phys. Rev. Lett. **104**, 066802 (2010).
[18] K. Ishizaka, M. S. Bahramy, H. Murakawa, M. Sakano, T. Shimojima, T. Sonobe, K. Koizumi, S. Shin, H. Miyahara, A. Kimura *et al.*, Nat. Mater. **10**, 521 (2011).
[19] S. V. Eremeev, I. A. Nechaev, Y. M. Koroteev, P. M. Echenique, and E. V. Chulkov, Phys. Rev. Lett. **108**, 246802 (2012).
[20] S. V. Eremeev, I. A. Nechaev, and E. V. Chulkov, JETP Lett. **96**, 437 (2012).
[21] M. Sakano, M. S. Bahramy, A. Katayama, T. Shimojima, H. Murakawa, Y. Kaneko, W. Malaeb, S. Shin, K. Ono, H. Kumigashira *et al.*, Phys. Rev. Lett. **110**, 107204 (2013).
[22] J. Luo, H. Munekata, F. F. Fang, and P. J. Stiles, Phys. Rev. B **41**, 7685 (1990).
[23] J. Nitta, T. Akazaki, H. Takayanagi, and T. Enoki, Phys. Rev. Lett. **78**, 1335 (1997).
[24] C. Quarti, E. Mosconi, and F. De Angelis, Chem. Mater. **26**, 6557 (2014).
[25] D. Niesner, M. Wilhelm, I. Levchuk, A. Osvet, S. Shrestha, M. Batentschuk, C. Brabec, and T. Fauster, Phys. Rev. Lett. **117**, 126401 (2016).
[26] L. Fu, C. L. Kane, and E. J. Mele, Phys. Rev. Lett. **98**, 106803 (2007).
[27] D. Hsieh, D. Qian, L. Wray, Y. Xia, Y. S. Hor, R. J. Cava, and M. Z. Hasan, Nature (London) **452**, 970 (2008).
[28] Y. L. Chen, J. G. Analytis, J. H. Chu, Z. K. Liu, S. K. Mo, X. L. Qi, H. J. Zhang, D. H. Lu, X. Dai, Z. Fang *et al.*, Science **325**, 178 (2009).
[29] S. V. Eremeev, Y. M. Koroteev, and E. V. Chulkov, JETP Lett. **91**, 387 (2010).
[30] A. Bansil, H. Lin, and T. Das, Rev. Mod. Phys. **88**, 021004 (2016).
[31] S. V. Eremeev, I. V. Silkin, T. V. Menshchikova, A. P. Protogenov, and E. V. Chulkov, JETP Lett. **96**, 780 (2013).
[32] D. Niesner, T. Fauster, S. V. Eremeev, T. V. Menshchikova, Y. M. Koroteev, A. P. Protogenov, E. V. Chulkov, O. E. Tereshchenko, K. A. Kokh, O. Alekperov *et al.*, Phys. Rev. B **86**, 205403 (2012).
[33] J. A. Sobota, S. L. Yang, A. F. Kemper, J. J. Lee, F. T. Schmitt, W. Li, R. G. Moore, J. G. Analytis, I. R. Fisher, P. S. Kirchmann *et al.*, Phys. Rev. Lett. **111**, 136802 (2013).
[34] S. Å. Lindgren and L. Walldén, Phys. Rev. Lett. **59**, 3003 (1987).
[35] T.-C. Chiang, Surf. Sci. Rep. **39**, 181 (2000).
[36] T. Torsti, V. Lindberg, M. J. Puska, and B. Hellsing, Phys. Rev. B **66**, 235420 (2002).
[37] A. M. Shikin, A. A. Rybkina, M. V. Rusinova, I. I. Klimovskikh, A. G. Rybkin, E. V. Zhizhin, E. V. Chulkov, and E. E. Krasovskii, New J. Phys. **15**, 125014 (2013).

[38] Y. Wu and Z. Li, Phys. Lett. A **378**, 2640 (2014).
[39] A. Varykhalov, D. Marchenko, M. R. Scholz, E. D. L. Rienks, T. K. Kim, G. Bihlmayer, J. Sánchez-Barriga, and O. Rader, Phys. Rev. Lett. **108**, 066804 (2012).
[40] R. L. H. Freire, A. Kiejna, and J. L. F. Da Silva, J. Phys. Chem. C **118**, 19051 (2014).
[41] S. H. Ahn, H. Tan, M. Haensch, Y. Liu, L. A. Bendersky, and T. P. Moffat, Energy and Environ. Sci. **8**, 3557 (2015).
[42] S. Štrbac, I. Srejić, and Z. Rakočević, J. Electrochem. Soc. **165**, J3335 (2018).
[43] X. Bokhimi, R. Zanella, and C. Angeles-Chaves, J. Phys. Chem. C **114**, 14101 (2010).
[44] Y.-J. Song, Y. M. López-De Jesús, P. T. Fanson, and C. T. Williams, J. Phys. Chem. C **117**, 10999 (2013).
[45] Y. Guan and E. J. M. Hensen, J. Catal. **305**, 135 (2013).
[46] Y.-J. Song, Y. M. López-De Jesús, P. T. Fanson, and C. T. Williams, Appl. Catal. B **154-155**, 62 (2014).
[47] H. A. Rojas, J. J. Matrínez, G. Díaz, and A. Gómez-Cortés, Appl. Catal. A **503**, 196 (2015).
[48] A. Aguilar-Tapia, R. Zanella, C. Calers, C. Loouis, and L. Delannoy, Phys. Chem. Chem. Phys. **17**, 28022 (2015).
[49] S. H. Park, H. M. Park, S. S. Han, S. Y. Han, and J. Y. Song, RSC Adv. **6**, 3210 (2016).
[50] K. Kusada, D. Wu, T. Yamamoto, T. Toriyama, S. Matsumura, W. Xie, M. Koyama, S. Kawaguchi, Y. Kubota, and H. Kitagawa, Chem. Sci. **10**, 652 (2019).
[51] T.-F. Zhang, S. M. Driver, S. J. Pratt, and D. A. King, Surf. Sci. **615**, 1 (2013).
[52] T.-F. Zhang, S. M. Driver, S. J. Pratt, S. J. Jenkins, and D. A. King, Surf. Sci. **648**, 10 (2016).
[53] M. M. Özer, C.-Z. Wang, Z.-Y. Zhang, and H. H. Weitering, J. Low Temp. Phys. **157**, 221 (2009).
[54] I. V. Silkin, Y. M. Koroteev, P. M. Echenique, and E. V. Chulkov, Materials **10**, 1409 (2017).
[55] G. Kresse and J. Furthmüller, Comput. Mat. Sci. **6**, 15 (1996).
[56] G. Kresse and J. Furthmüller, Phys. Rev. B **54**, 11169 (1996).
[57] D. M. Ceperley and B. J. Alder, Phys. Rev. Lett. **45**, 566 (1980).
[58] H. J. Monkhorst and J. D. Pack, Phys. Rev. B **13**, 5188 (1976).
[59] H. Wolfschmidt, C. Baier, S. Gsell, M. Fischer, M. Schreck, and U. Stimming, Materials **3**, 4196 (2010).
[60] J. W. Arblaster, Platinum Metals Rev. **54**, 93 (2010).
[61] J. Courtois, W. Du, E. Wong, X. Teng, and N. A. Deskins, Appl. Cat. A **483**, 85 (2014).
[62] A. V. Ruban, H. L. Skriver, and J. K. Nørskov, Phys. Rev. B **59**, 15990 (1999).
[63] E. E. Krasovskii, Phys. Rev. B **90**, 115434 (2014).
[64] E. V. Chulkov, V. M. Silkin, and P. M. Echenique, Surf. Sci. **437**, 330 (1999).
[65] C. Corriol, V. M. Silkin, D. Sanchez-Portal, A. Arnau, E. V. Chulkov, P. M. Echenique, T. von Hofe, J. Kliewer, J. Kröger, and R. Berndt, Phys. Rev. Lett. **95**, 176802 (2005).
[66] Y. M. Koroteev and E. V. Chulkov, Adv. Quantum Chem. **80**, 175 (2019).
[67] R. Mazzarello, A. Dal Corso, and E. Tosatti, Surf. Sci. **602**, 893 (2008).
[68] R. Requist, P. M. Sheverdyaeva, P. Moras, S. K. Mahatha, C. Carbone, and E. Tosatti, Phys. Rev. B **91**, 045432 (2015).
[69] J. Henk, M. Hoesch, J. Osterwalder, A. Ernst, and P. Bruno, J. Phys.: Condens. Matter **16**, 7581 (2004).
[70] N. L. Zaitsev, R. Tonner, and I. A. Nechaev, J. Phys.: Condens. Matter **31**, 204001 (2019).
[71] S. L. Hulbert, P. D. Johnson, and M. Weinert, Phys. Rev. B **34**, 3670 (1986).
[72] S. D. Kevan and R. H. Gaylord, Phys. Rev. B **36**, 5809 (1987).
[73] P. Roos, E. Bertel, and K. D. Rendulic, Chem. Phys. Lett. **232**, 537 (1995).
[74] A. Schäfer, I. L. Shumay, M. Wiets, M. Weinelt, T. Fauster, E. V. Chulkov, V. M. Silkin, and P. M. Echenique, Phys. Rev. B **61**, 13159 (2000).
[75] S. Link, H. A. Durr, G. Bihlmayer, S. Blügel, W. Eberhardt, E. V. Chulkov, V. M. Silkin, and P. M. Echenique, Phys. Rev. B **63**, 115420 (2001).
[76] J. Wiebe, F. Meier, K. Hashimoto, G. Bihlmayer, S. Blügel, P. Ferriani, S. Heinze, and R. Wiesendanger, Phys. Rev. B **72**, 193406 (2005).
[77] I. E. Tamm, Z. Phys. **76**, 849 (1932).
[78] A. Urru and A. Dal Corso, Surf. Sci. **671**, 17 (2018).
[79] A. Dal Corso, Surf. Sci. **637-638**, 106 (2015).
[80] E. Starodub, A. Bostwick, L. Moreschini, S. Nie, F. E. Gabaly, K. F. McCarty, and E. Rotenberg, Phys. Rev. B **83**, 125428 (2011).
[81] I. Pletikosić, M. Kralj, D. Šokçević, R. Brako, P. Lazić, and P. Pervan, J. Phys.: Condens. Matter **22**, 135006 (2010).
[82] P. Pervan, P. Lazić, M. Petrović, I. Šrut Rakić, I. Pletikosić, M. Kralj, M. Milun, and T. Valla, Phys. Rev. B **92**, 245415 (2015).
[83] J. Sánchez-Barriga, G. Bihlmayer, D. Wortmann, D. Marchenko, O. Rader, and A. Varykhalov, New J. Phys. **15**, 115009 (2013).
[84] H. J. Elmers, D. Kutnyakhov, S. V. Chernov, K. Medjanik, O. Fedchenko, A. Zaporozhchenko-Zymakova, M. Ellguth, C. Tusche, J. Viefhaus, and G. Schönhense, J. Phys.: Condens. Matter **29**, 255001 (2017).